Int. J. Heat Mass Transfer. Vol. 33, No. 3, pp. 555–570, 1990
Printed in Great Britain

0017–9310/90 $3.00 + 0.00

Regions of heat transfer enhancement for laminar mixed convection in a parallel plate channel

J. R. MAUGHAN† and F. P. INCROPERA
Heat Transfer Laboratory, School of Mechanical Engineering, Purdue University, West Lafayette, IN 47907, U.S.A.

(*Received* 27 *February* 1989 *and in final form* 7 *July* 1989)

Abstract—Heat transfer enhancement in mixed convection flow between parallel plates heated uniformly from below is investigated. Numerical computations demonstrate heat transfer enhancement prior to the onset of thermal instability in a horizontal channel due to fluid expansion and an induced pressure gradient, and in an inclined channel due to the component of gravity in the flow direction. Flow visualization and heat transfer measurements for airflow in a horizontal channel are performed over a wide range of conditions to delineate regions of forced and mixed convection. The onset of secondary flow is found to precede appreciable heat transfer enhancement. Except for large values of Gr^*/Re^2, Nusselt numbers prior to the onset of enhancement may be predicted with forced convection correlations. Thereafter, Nusselt numbers rise rapidly to a maximum value and then assume a fully developed value which is slightly lower than the maximum. Correlations are suggested for the fully developed Nusselt numbers and for the locations of the onset of secondary flow, the onset of enhancement, and the maximum Nusselt number.

1. INTRODUCTION

THE THERMAL instability associated with convection between two heated plates can result in buoyancy-driven secondary flows and appreciable heat transfer enhancement. Consequently, mixed convection can occur in systems ranging from chemical vapor deposition and heat exchangers to flow between printed circuit boards. In each case it is important to know whether secondary flows and heat transfer enhancement can be expected.

Mixed convection in the entry region between heated plates is characterized by an upstream region of thin boundary layers and stable, forced convection. As the growing thermal boundary layer destabilizes, a region of developing secondary flow begins and heat transfer coefficients rise above forced convection levels. Eventually, a fully developed condition of buoyancy-driven plumes and vortices can result, with Nusselt numbers several times higher than those expected for fully developed, laminar forced convection. In addition, for large heat rates and low flow rates, or for an inclined channel, buoyancy forces can enhance heat transfer prior to the onset of instability.

Early research on laminar ($Re < 1000$) mixed convection between parallel plates [1, 2] involved fully developed flow between horizontal, isothermal plates. With the bottom plate heated and the upper plate cooled, secondary flow and heat transfer enhancement were found to occur for $Ra > 1708$, as predicted for Rayleigh–Benard thermal instability. Furthermore, Nusselt numbers in the fully developed region were independent of the flow rate. For low Rayleigh numbers ($Ra < 10\,000$), the secondary flow consisted of laminar longitudinal vortices, while higher Rayleigh numbers resulted in transition of the laminar vortex structure to a condition more typical of turbulent free convection.

Subsequent work on mixed convection between plates [3, 4] investigated inlet conditions by introducing smoke into the thermal entry region and noting the onset of secondary flow. Although there was some scatter in the data, results were scaled with Ra_c and z_c^* and clearly showed that the onset of instability moved upstream with increasing plate temperature and decreasing flow rate. As expected, measured critical Rayleigh numbers were considerably higher than theoretical predictions [5]. Longitudinal distributions of measured heat transfer coefficients in the thermal entry region [4] showed a monotonic decay in the forced convection region before leveling off to a fully developed value. Other investigators [6, 7] used laser Doppler anemometry to identify changes in velocity profiles that would mark the establishment of a secondary flow. They also attempted to identify the channel length required to achieve fully developed conditions. Although the results were not compared to data from earlier studies, the conclusions and trends were qualitatively similar.

Subsequent studies of the longitudinal Nusselt number distribution in the thermal entry region [8, 9] improved the spatial resolution of the data by measuring temperature distributions on a uniformly heated bottom surface. The upper surface was well insulated. As found in the earlier study with isothermal plates [4], heat transfer coefficients decayed monotonically in the forced convection region. However, for uniform bottom heating, the Nusselt number experienced a minimum near the onset of instability and subsequent downstream oscillations. Accompanying flow visu-

† Present address: General Electric Corporate Research and Development, Schenectady, NY 12301, U.S.A.

NOMENCLATURE

g	acceleration due to gravity
Gr	Grashof number, $g\beta\Delta TH^3/\nu^2$
Gr^*	modified Grashof number, $g\beta qH^4/k\nu^2 = Gr\ Nu$
h	heat transfer coefficient, $q/(T_s - T_b)$
H	channel height or plate separation
k	thermal conductivity
Nu	Nusselt number, hH/k
p	pressure
Pe	Peclet number, $Re\ Pr$
Pr	Prandtl number, ν/α
q	heat rate per area, heat flux
Ra	Rayleigh number, $Gr\ Pr = g\beta\Delta TH^3/\nu\alpha$
Ra^*	modified Rayleigh number, $Gr^*\ Pr = g\beta qH^4/k\nu\alpha$
Re	Reynolds number, $\bar{w}H/\nu$
T	temperature
ΔT	temperature difference
u, v, w	spanwise, vertical, and axial velocity
$\bar{w}$	mean axial velocity
x, y, z	spanwise, vertical, and axial coordinate
z^*	non-dimensional axial distance, $z/(H\ Re\ Pr)$.

Greek symbols

α	thermal diffusivity
β	coefficient of thermal expansion
ε	emissivity
θ	inclination angle from horizontal
Θ	non-dimensional temperature
ν	kinematic viscosity
ρ	density.

Subscripts

b	bulk value (bulk temperature)
c	critical value at onset of instability
f	forced convection value; also critical value based on flow visualization
fd	fully developed value or condition
h	critical value based on heat transfer data
in	inlet value
max	maximum value or location of maximum value
s	surface value
t	turbulence or location of turbulence.

alization [8, 10] revealed four flow regimes which progressed from laminar forced convection (no secondary flow), laminar mixed convection (secondary flow characterized by steady longitudinal vortices and plumes), a transitional region of unsteady flow and increasingly distorted flow structures, and a terminal region exhibiting unsteady conditions typical of turbulent free convection. Heat transfer measurements performed as a function of channel inclination [9] revealed that, with increasing inclination angle (from the horizontal), onset of the secondary flow was delayed and that, prior to onset, there was appreciable heat transfer enhancement due to flow acceleration caused by the component of gravity in the flow direction.

Mixed convection in a horizontal channel prior to the onset of secondary flow has been considered numerically [11], and it was demonstrated that buoyancy forces can affect velocity and temperature profiles and enhance heat transfer. Although no physical explanation was given, the effect can be attributed to an induced longitudinal pressure gradient first described for flow over a horizontal flat plate [12]. The thicker thermal boundary layer over downstream sections of the heated plate causes the weight of the fluid, and therefore the pressure, to be slightly reduced, resulting in a favorable axial pressure gradient, flow acceleration, and heat transfer enhancement. Calculations for pre-instability enhancement in an inclined channel were not considered in ref. [11]. Many of the noted effects of mixed convection in a channel also characterize mixed convection flow over a heated flat plate, including longitudinal plumes and vortices [13], oscillations in the Nusselt number distribution [14], and pre-instability enhancement on an inclined surface [15].

Although many phenomena related to mixed convection in channels are well understood, uncertainty remains concerning the effect of flow, thermal and geometric parameters on their occurrence and their impact on heat transfer. This work builds on previous research by the authors [8–10] by focusing on pre-instability heat transfer enhancement, locations corresponding to the onset of secondary flow, post-instability heat transfer enhancement and fully developed conditions, and on the correlation of fully developed Nusselt numbers. Hence, the primary objective of this study is to quantitatively delineate the different flow regimes and to assess the influence of buoyancy on heat transfer enhancement in each regime. Results from a numerical analysis of pre-instability heat transfer enhancement will be presented first and will be followed by experimental results that cover a wide range of parameters and can be used to identify regions of interest.

2. ANALYSIS OF PRE-INSTABILITY HEAT TRANSFER ENHANCEMENT

2.1. *Model and numerical procedures*

To assess the range and magnitude of pre-instability heat transfer enhancement in a channel, a numerical

investigation of two-dimensional mixed convection was undertaken. The analysis was conducted for horizontal and inclined channels heated uniformly from below, and emphasis was placed on identifying parameters which can be used to predict heat transfer enhancement for a wide range of conditions. Plate conduction effects were neglected, and the thermal entry region was investigated by prescribing laminar fully developed flow at the start of the heated section.

Assuming steady, two-dimensional, laminar flow with constant properties and the Boussinesq approximation, the appropriate governing equations can be nondimensionalized to obtain

$$\frac{\partial v^*}{\partial y^*} + \frac{\partial w^*}{\partial z^*} = 0 \tag{1}$$

$$v^* \frac{\partial v^*}{\partial y^*} + w^* \frac{1}{Pr} \frac{\partial v^*}{\partial z^*} = -Re^2 \frac{\partial p^*}{\partial y^*} + \frac{\partial^2 v^*}{\partial y^{*2}} + \frac{1}{Pe^2} \frac{\partial^2 v^*}{\partial z^{*2}} + \cos\theta \frac{Gr^*}{Pr} \Theta \tag{2}$$

$$v^* \frac{\partial w^*}{\partial y^*} + w^* \frac{1}{Pr} \frac{\partial w^*}{\partial z^*} = -\frac{1}{Pr} \frac{\partial p^*}{\partial z^*} + \frac{\partial^2 w^*}{\partial y^{*2}} + \frac{1}{Pe^2} \frac{\partial^2 w^*}{\partial z^{*2}} + \sin\theta \frac{Gr^*}{Re} \Theta \tag{3}$$

$$Pr\, v^* \frac{\partial \Theta}{\partial y^*} + w^* \frac{\partial \Theta}{\partial z^*} = \frac{\partial^2 \theta}{\partial y^{*2}} + \frac{1}{Pe^2} \frac{\partial^2 \Theta}{\partial z^{*2}} \tag{4}$$

where

$$y^* = \frac{y}{H}, \quad z^* = \frac{z}{H\, Re\, Pr} \tag{5a}$$

$$v^* = \frac{v}{v/H}, \quad w^* = \frac{w}{\tilde{w}} \tag{5b}$$

$$p^* = \frac{p}{\rho \tilde{w}^2} \tag{5c}$$

$$\Theta = \frac{T - T_{in}}{q(H/k)}. \tag{5d}$$

The boundary conditions are

$$y^* = 0: \quad v^* = 0, \quad w^* = 0, \quad \frac{\partial \Theta}{\partial y^*} = -1 \tag{6a}$$

$$y^* = 1: \quad v^* = 0, \quad w^* = 0, \quad \frac{\partial \Theta}{\partial y^*} = 0 \tag{6b}$$

$$z^* = 0: \quad v^* = 0, \quad w^* = 6(y^* - y^{*2}), \quad \Theta = 0 \tag{6c}$$

$$z^* = L/(H\, Re\, Pr): \quad \frac{\partial v^*}{\partial z^*} = 0, \quad \frac{\partial w^*}{\partial z^*} = 0, \quad \frac{\partial \Theta}{\partial z^*} = 1. \tag{6d}$$

The outflow boundary condition is exact only for flows which become fully developed. To ensure that Nusselt numbers in the entry region were insensitive to this outflow assumption, the channel length was extended well beyond the region of interest.

Further insight into pertinent physical mechanisms can be obtained by making additional approximations for the v-momentum equation and substituting it into the w-momentum equation. Anticipating conditions for which terms involving Gr^* and Re are much larger than the remaining v^* terms, equation (2) simplifies to

$$Re^2 \frac{\partial p^*}{\partial y^*} = \cos\theta \frac{Gr^*}{Pr} \Theta. \tag{7}$$

Integrating over y^* and differentiating with respect to z^*, it follows that

$$\frac{\partial p^*}{\partial z^*} = \left.\frac{\partial p^*}{\partial z^*}\right|_{y^*=1} - \cos\theta \frac{Gr^*}{Re^2\, Pr} \left[\frac{\partial}{\partial z^*} \int_{y^*}^{1} \Theta \, dy^*\right]. \tag{8}$$

Hence, substituting into equation (2)

$$v^* \frac{\partial w^*}{\partial y^*} + w^* \frac{1}{Pr} \frac{\partial w^*}{\partial z^*} = -\frac{1}{Pr} \left.\frac{\partial p^*}{\partial z^*}\right|_{y^*=1} + \cos\theta \frac{Gr^*}{(Re\, Pr)^2} \frac{\partial}{\partial z^*} \int_{y^*}^{1} \Theta \, dy^* + \frac{\partial^2 w^*}{\partial y^{*2}} + \frac{1}{Pe^2} \frac{\partial^2 w^*}{\partial z^{*2}} + \sin\theta \frac{Gr^*}{Re} \Theta. \tag{9}$$

This approximate axial momentum equation reveals the different mechanisms associated with flow in the streamwise direction. The term $(\sin\theta\,(Gr^*/Re))\Theta$ represents the component of gravity which is parallel to the surface and directly accelerates flow in the z-direction. However, acceleration is augmented by the term

$$\cos\theta \frac{Gr^*}{(Re\, Pr)^2} \frac{\partial}{\partial z^*} \int_{y^*}^{1} \Theta \, dy^*.$$

Since Θ is positive, the value of the integral is positive, and with Θ proportional to $T - T_{in}$, the value of the integral increases as plate and fluid temperatures increase. Hence, the term is positive and acts as a negative pressure gradient, thereby also contributing to flow acceleration. Alternatively, this acceleration can be viewed as a result of fluid expansion within the channel. Hence, there are two mechanisms for fluid acceleration due to buoyancy forces: (i) direct acceleration which scales with $\sin\theta\,(Gr^*/Re)$, and (ii) indirect acceleration caused by the induced pressure gradient, which scales with $\cos\theta\,(Gr^*/(Re\, Pr)^2)$. Although combining the v-momentum equation into the axial equation helps clarify the flow mechanisms, all the calculations were performed using the full set of equations (1)–(4).

For $\theta = 0°$ (horizontal channel) buoyancy acts only through the induced negative pressure gradient; for $\theta = 90°$ (vertical channel), it acts only through the direct acceleration. At intermediate inclinations, both mechanisms are active, although direct acceleration is expected to be more important. In order to assess

their relative magnitudes, the two effects were initially considered separately.

Finite-difference calculations were performed using the SIMPLER procedure [16]. Twenty-five nodes were placed along the height of the channel, with 50 nodes in the axial direction. Nodes were concentrated near the heated surface and upstream regions of the channel. This nodal resolution was sufficient to give grid independent results for $Gr^* > 0$ and excellent agreement with the analytical forced convection solution when calculations were performed for $Gr^* = 0$. All of the results were scaled with z^* and, since the behavior of Nu_f with z^* is well known [17], are displayed in terms of the parameter Nu/Nu_f, which expresses the local heat transfer enhancement due to pre-instability mixed convection effects. Calculations were performed for $Pe = 200$, which was sufficiently large to ensure that further increases in Pe had no effect on the variation of the Nusselt number with z^*.

2.2. *Numerical results*

Numerical results describing the effects of direct acceleration on heat transfer for an inclined channel are given in Fig. 1, which is completely applicable for a vertical channel but represents only one component of enhancement for an inclined channel. Heat transfer enhancement increases with dimensionless axial distance (initially) and with the scaling parameter $\sin\theta\,(Gr^*/Re)$. Thus, as expected, this effect is more pronounced for large angles of inclination, high heat fluxes, and low flow rates. At $z^* \approx 0.2$, the Nusselt number achieves a fully developed value, as the combined pressure, buoyancy, and viscous forces reach equilibrium. Because of numerical instability at large values of $\sin\theta\,(Gr^*/Re)$, not every calculation could be extended to $z^* = 1.0$.

Similar results for the induced pressure gradient effect are shown in Fig. 2. The results are fully applicable to a horizontal channel, but account for only one component of the total acceleration in an inclined channel. Again, enhancement increases with z^* and the appropriate scaling parameter, $\cos\theta\,(Gr^*/Re^2)$. Fully developed conditions do not exist for this case since the uniform heat flux boundary condition continuously increases the fluid temperature, thereby increasing fluid expansion and acceleration. Theoretically, it would be possible to choke the flow through heat transfer, although the two-dimensional assumption upon which these calculations are based would be valid only for relatively small levels of enhancement.

The absence of fully developed conditions contrasts sharply with results obtained for horizontal isothermal plates, with the bottom plate heated and the upper plate cooled. Since the plates are each at a uniform temperature, a fully developed state quickly develops, where the fluid temperature profile no longer changes, either in terms of its shape or magnitude. Since there is no axial temperature gradient, the buoyancy-induced pressure gradient dissipates and the acceleration and enhancement decay to zero.

The two pre-instability mixed convection effects

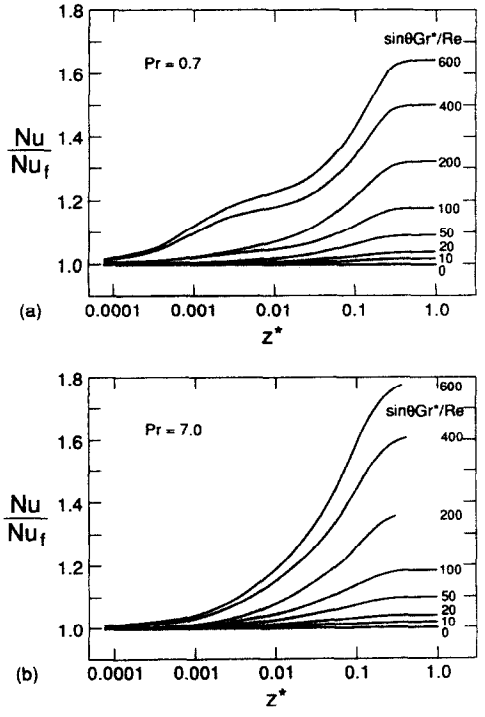

FIG. 1. Pre-instability heat transfer enhancement caused by direct acceleration.

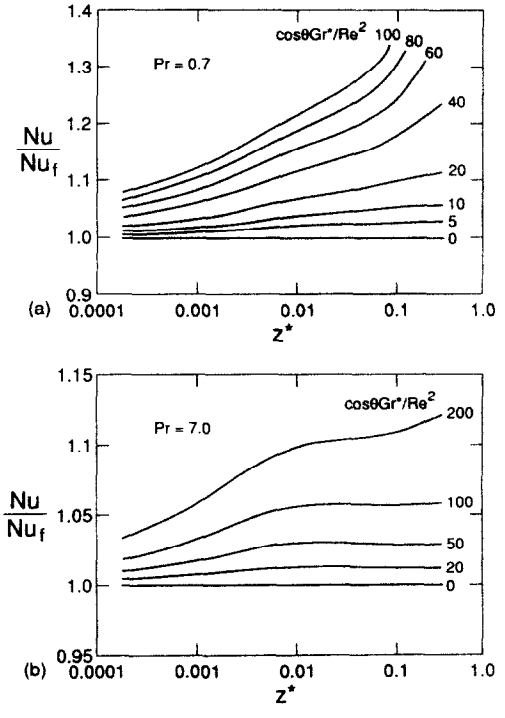

FIG. 2. Pre-instability heat transfer enhancement caused by indirect acceleration or induced pressure gradient.

have been clarified through separate consideration. However, in an inclined channel, both mechanisms are present, although, for all but the smallest angles of inclination, $\sin\theta\,(Gr^*/Re) \gg \cos\theta\,(Gr^*/Re^2)$ and direct acceleration is dominant. As an approximation, the separate effects may be simply added for conditions where neither is dominant. However, it is important to note that the laminar two-dimensional model is very restrictive in view of other physical processes occurring in the channel. In particular, before this type of enhancement can progress too far, the flow may become thermally unstable, rendering the model assumptions invalid. Hence, although the foregoing results call attention to these processes and predict their effects, the limitations of the model assumptions must be kept clearly in mind.

3. EXPERIMENTAL PROCEDURES

3.1. *Apparatus and procedure*

Experiments were performed using the horizontal air channel shown schematically in Fig. 3. Ambient air is drawn into the blower, metered and conditioned before passing through the channel. Warm air leaving the blower is cooled to ambient temperature with a compact air-to-water heat exchanger. The inlet temperature of the water is controlled by the data acquisition computer which, acting on input provided by thermocouples in the airstream leaving the exchanger, opens or closes an electronically-controlled valve mixing hot and cold water. A uniform and constant inlet temperature is assured with an additional heat exchanger located just prior to the channel entrance. This exchanger is driven by a constant temperature bath held at the ambient temperature of the laboratory.

The boundary conditions were a uniformly heated bottom surface (uniform heat flux) and an adiabatic upper surface. As described previously [9], the uniform heat flux was provided by a stainless steel foil heater, extensively instrumented with thermocouples. The upper surface was 6.35 mm plate glass. The channel had a fixed width of 305 mm and a test section length of 881 mm, but had several sets of sidewalls which could be interchanged to provide channel heights of approximately 15–60 mm. The entire channel was well insulated with 350 mm of Styrofoam and fiberglass insulation.

The heated air leaving the channel was discharged freely and then drawn away and vented to the outside ambient with another blower. This procedure maintained the air pressure in the channel close to ambient and reduced the sensitivity of flow conditions to variations in outside air pressure.

The system used to generate smoke for flow visualization is also shown in Fig. 3. The aerosol generator emits a dispersion of very fine oil particles (dioctylphthalate), which are small enough to track the slowly moving fluid in the channel but also scatter light and are easily photographed. This vapor can be diluted with additional air and then proportioned between injection into the channel or ventilation to the exhaust. Smoke was injected into the channel through a slot machined across the width of the heater plate in a manner similar to that used previously in water [10]. A uniform layer of smoke could be injected into the bottom of the boundary layer, broken only by spacers in the slot placed at 25.4 mm intervals, and the injection rate could be adjusted until there was no discernible disturbance to the flow. When illuminated through the sidewalls by two fluorescent lamps and viewed from above through the glass plate, a sharp contrast could be achieved between the heater surface, which reflects little light toward the observer, and the smoke, which scatters light well.

The following procedures were used to obtain the data. After assembling, leveling, and cleaning the channel, its height was carefully measured, the insulation was installed, and the flow rate and heat flux

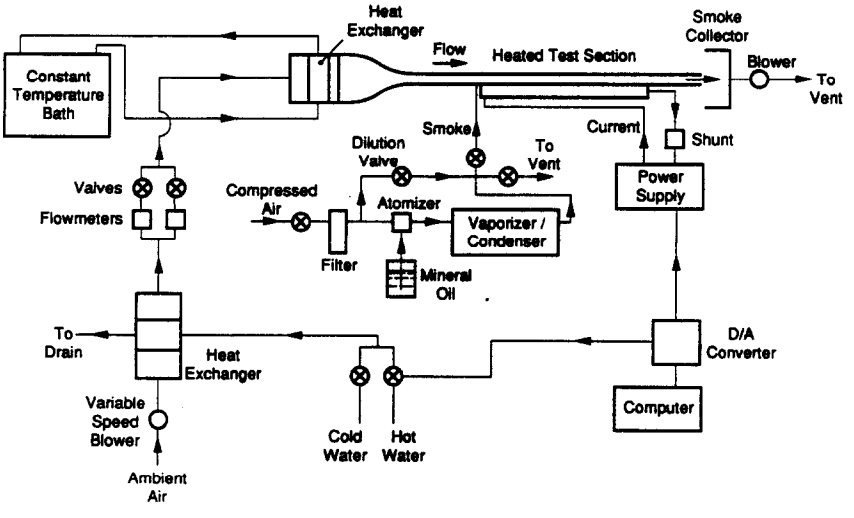

FIG. 3. Schematic of experimental apparatus.

were fixed. Parameters such as the plate-averaged Nusselt number were monitored until steady state conditions were achieved, which took from 6–16 h. After conditions had been steady for some time (2–3 h), plate temperatures and all other data were taken 10 times at 30 s intervals, averaged, and stored.

Flow visualization immediately followed acquisition of the heat transfer data. To prepare the channel for flow visualization, sections of insulation on either side of the channel were removed and replaced by the fluorescent lamps. The smoke generator was activated, and the injection rate was adjusted until sufficient smoke was visible. A cut-out section of the insulation above the top plate was then removed, leaving the heated surface visible through the glass plate. Two photographs were taken at 10 s intervals, after which the smoke generator was then deactivated and the channel insulation restored.

Heat transfer data are reported as spanwise-averaged Nusselt numbers, where the local Nusselt number at each measurement station is defined as $Nu = qH/(T_s - T_b)k$. The local surface temperature was obtained from the thermocouple measurement, while the local bulk temperature was determined from an energy balance which accounted for heat losses to the surroundings. The convective flux q was calculated by correcting energy dissipation in the foil for conduction and radiation losses. Radiation heat transfer from the surface was calculated from the assumption of two isothermal, infinite, parallel plates. Comparison to calculations from a more rigorous, zonal model for specular radiation transfer showed the simple model to be adequate (<1% error). Conduction losses through the insulation were determined by measuring the temperature drop across the insulation underlying the heater plate. As discussed previously [9], axial conduction effects were limited to the first few centimeters of the plate, and spanwise conduction was neglected.

3.2. *Uncertainty and validation*

Uncertainties in the Nusselt number (and other parameters) were estimated according to standard procedures [9]. Hence, although each individual measurement from which Nu was determined is believed to be accurate to better than 1%, the combination of many measurements, together with uncertainties in predicted quantities (radiation and conduction losses) and neglected (conjugate) effects, yields Nusselt number uncertainties from 6–10% for small to moderate channel heights, and of approximately 20% for the largest channel height (60 mm), which is characterized by the lowest heat transfer coefficients.

The greatest contribution to the uncertainty comes from the plate emissivity, which was measured as $\varepsilon = 0.10 \pm 0.03$, or to within 30%. A 30% uncertainty in the correction for radiation in a situation where radiation losses are 30% contributes an uncertainty of nearly 10% in the convective heat flux, and therefore in the Nusselt number. Uncertainty in the modified Grashof number, Gr^*, ranged from 7–30%, which primarily reflects uncertainty in the convective heat flux and in the channel height. The estimated uncertainty in the Reynolds number was 2%. Because of fluid property variations with temperature, Re and Gr^* vary with axial distance, and although variations in the Reynolds number were small (<5%), the Grashof number could vary by as much as 30%. Variations in Gr^* are more pronounced because non-uniform radiation and convection losses cause variations in the local convective heat flux. For convenience, experiments are identified according to Reynolds and Grashof numbers based on inlet conditions and the total dissipated flux, while graphical results involving the Grashof or Rayleigh number are based on the local bulk temperature and local convective heat flux.

The reliability of the data was established through various tests and comparisons with appropriate standard conditions. The most relevant comparison is with the analytical solution for forced convection between horizontal parallel plates with uniform heat flux at the bottom and an adiabatic upper surface [17]. The comparison is made in Fig. 4 for six different data sets, with heat fluxes sufficiently low to ensure forced convection conditions. In downstream regions, agreement is excellent and well within the experimental uncertainty. The depressed experimental Nusselt numbers on the extreme upstream portion of the plate are due to the effects of axial conduction in the heater assembly.

The possible influence of smoke injection on secondary flows within the channel was indirectly assessed by noting changes in the heat transfer data over an extended period of flow visualization. Injecting smoke into the channel for a period of 1.5 h had no noticeable effect on the longitudinal Nusselt number distribution, while a test period of 6 h resulted in slightly higher measured Nusselt numbers in the forced convection region, but no changes in the location of the onset of instability or in the Nusselt numbers further downstream. Since a noticeable oil film had developed in the forced convection region over that period of time, the increase in Nu was attri-

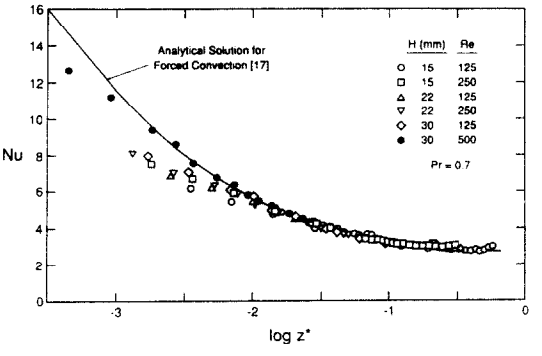

FIG. 4. Comparison of experimental results with analytical solution for forced convection in thermal entry region.

buted to an increase in the effective plate emissivity. The invariance of the heat transfer data to such extreme periods of smoke injection indicates that the flow visualization was not modifying the secondary flow.

4. EXPERIMENTAL RESULTS

Experiments were performed over the widest possible range of conditions. For each channel height and flow rate, heat fluxes ranged from the smallest value still providing measurable temperature differences (≈ 1 W m^{-2} corresponding to 0.5°C) to a maximum value limited by the need to hold plate temperatures under about 90°C (≈ 300 W m^{-2}). The lowest Reynolds number was limited by the turbine flow meters to 125, and the maximum was held to 500 to ensure laminar flow. The smallest channel height was 15 mm, which was just large enough to achieve secondary flow at the lowest measurable flow rate and highest allowable heat flux. Experiments considered the thermal entry region by allowing the laminar velocity profile to become fully developed before the heated test section.

For each condition, plate temperature measurements were recorded and top view photographs were taken, providing results similar to those shown in Fig. 5. From the photograph and Nusselt number distribution, secondary flow development can be contrasted with changes in the Nusselt number and compared to the analytical solution for forced convection. Initially, plate conditions are characteristic of laminar forced convection. The Nusselt number shows a sharp decay in accordance with the analytical prediction, and the photograph reveals that the smoke continues to move undisturbed along the heater surface. Pre-instability enhancement is not evident for this condition.

As the thermal boundary layer thickens, the effects of thermal instability become manifest through flow visualization near the position marked *onset of secondary flow*, where the smoke begins to coalesce into 8 or 10 plumes on the heater surface. The critical location associated with onset of the secondary flow, $z_{c,f}$, is determined by tracing the smoke to the point where it first appears to shift in the spanwise direction. Although the subjective nature of identifying the onset of secondary flow is minimized through this approach, the uncertainty in the location can still be large for some flow conditions, ranging from ± 10 to ± 80 mm. A typical value for the uncertainty in $z_{c,f}$ is $\pm 10\%$. Note that the heat transfer data at this axial location do not yet show any significant deviation from forced convection.

The effects of thermal instability on heat transfer are not evident until somewhat later, when the plumes are more fully established and the descending flow between plumes has gained strength. This location is termed the onset of heat transfer enhancement, as determined from the heat transfer data, or $z_{c,h}$. The value of $z_{c,h}$ was determined by looking for a sharp increase in the longitudinal distribution of Nu/Nu_f. This procedure provides a more precise measure of the onset point than simply associating onset with an arbitrarily selected value of Nu/Nu_f, since some of the apparent enhancement could be due to experimental uncertainty or to pre-instability enhancement mechanisms. The uncertainty in $z_{c,h}$ is approximately $\pm 10\%$. For every flow condition, $z_{c,h}$ is greater than $z_{c,f}$, thus establishing that developing secondary flows do not immediately cause significant heat transfer enhancement. Such early development moves fluid within the boundary layer but significant changes in the Nusselt number are delayed until the descending cool flow from the channel core reaches the plate and longitudinal convection cells become well established.

Continued strengthening of the convection cells causes the Nusselt number to continue to increase, until an initial maximum is reached at z_{max}. Beyond this point, the heat transfer coefficient decreases slightly and begins to show some oscillatory behavior, perhaps as fluid alternately recirculates between the cool core and warmer plate surface. Although it is not evident for the conditions of Fig. 5, continued development of the secondary flow is characterized by a decay in the oscillations and a fully developed Nusselt number. Furthermore, when flow visualization revealed that strong buoyancy forces were driving the secondary flow to turbulence, there was no apparent effect on the longitudinal Nusselt number distribution.

4.1. *Effect of heat flux, flow rate, channel height, and inclination*

Figures 6–9 summarize the effects of heat flux, flow rate, channel height, and inclination angle on mixed convection between parallel plates. The effect of heat flux on secondary flow development is revealed by the top view photographs of Fig. 5. Most noticeable is the advancement in the onset of instability as the Grashof number is increased, a trend which is also evident in the corresponding heat transfer data of Fig. 7(a). It is clear that the amount of heat transfer enhancement increases with heat flux (Fig. 7(a)), as does the number of plumes spaced across the heater plate (Fig. 5). Note that data for $Gr^* = 2.0 \times 10^5$ and 4.0×10^5 approach fully developed conditions. The apparent increase in Nu beginning near $z = 700$ mm can be attributed to increased radiation and conduction losses near the end of the heater plate. Figure 6 also shows that larger heat fluxes are associated with decay of the longitudinal cells to turbulence.

The data included in Fig. 7 show that, by increasing the Reynolds number, the onset of secondary flow moves downstream and may, in fact, not occur at all on the length of the heater plate. This effect is expected, as the increased flow velocity thins the boundary layer, thereby increasing its resistance to thermal instability and impeding secondary flow development.

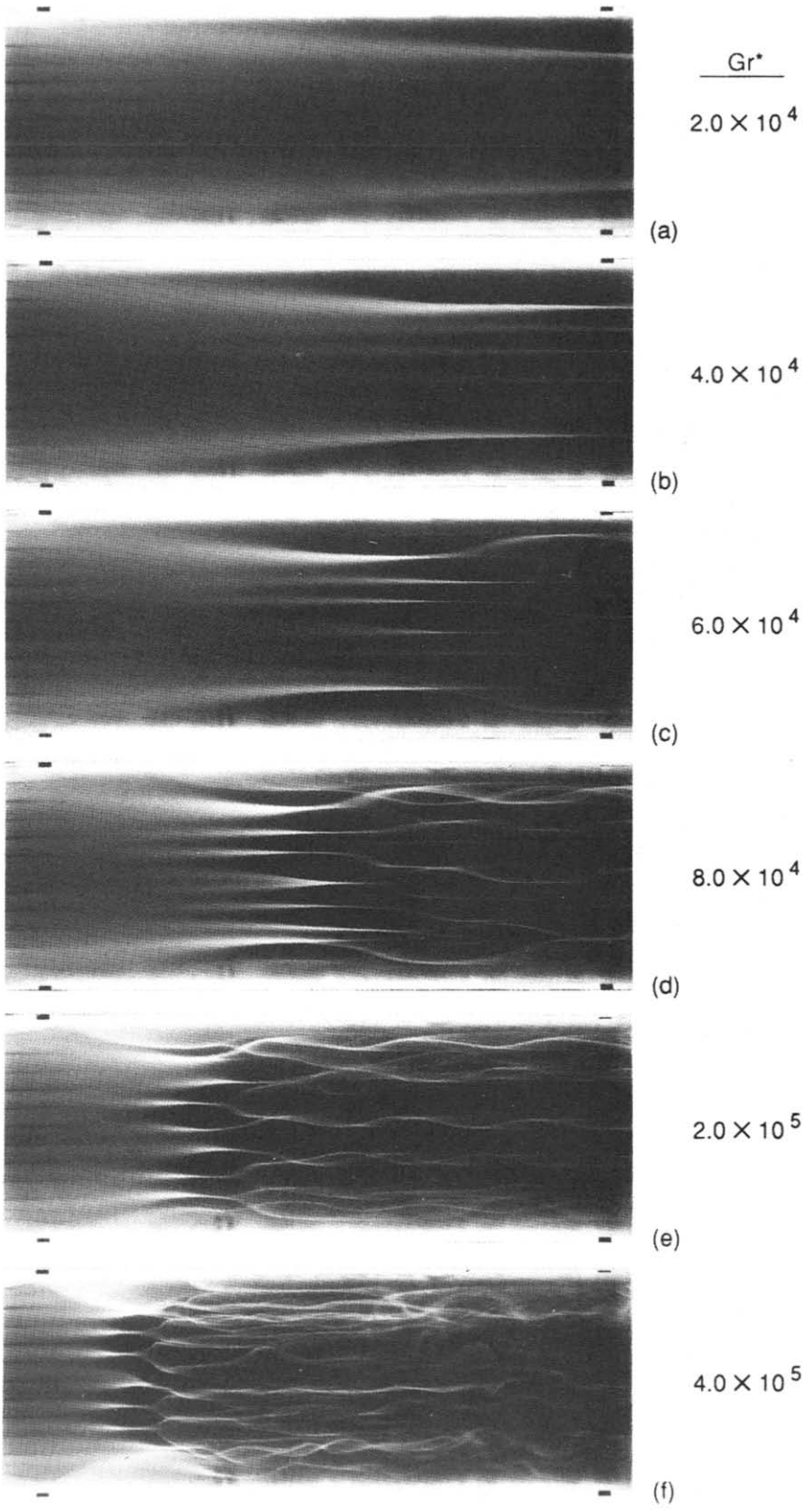

FIG. 5. Comparison of secondary flow development and longitudinal distribution of the Nusselt number.

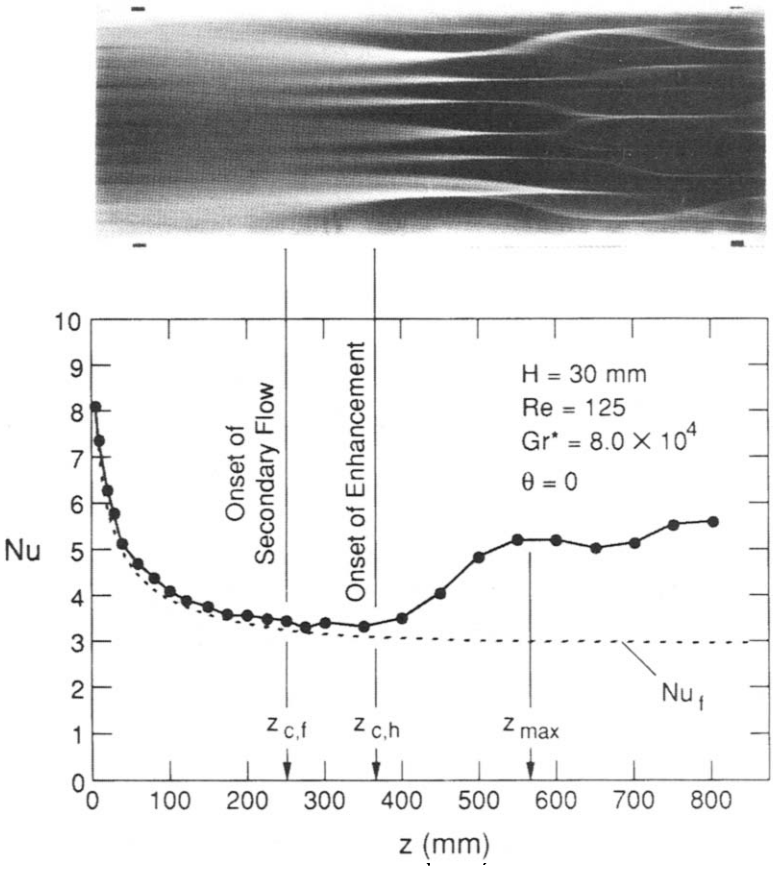

FIG. 6. Effect of Grashof number on secondary flow development for $H = 30$ mm, $Re = 125$, $Pr = 0.7$, and $\theta = 0°$.

Figure 8 shows that increasing the channel height has a very significant impact on mixed convection between parallel plates and encourages the development of secondary flows. For a fixed flow rate, the Reynolds number does not change as the height is increased, while, for a fixed heat flux, the modified Grashof number increases with channel height to the fourth power, or H^4. Hence, even a modest increase in plate separation results in much stronger secondary flows. An increase in channel height also reduces the aspect ratio of the channel, causing sidewall effects to become more important and reducing the likelihood of true parallel plate behavior.

From Fig. 9, it is evident that, by inclining the plate, the attendant buoyancy-assisting force has two effects. The effects are a delay in the onset of thermal instability and heat transfer enhancement prior to the onset of secondary flow. Both effects are due to acceleration of the flow by the component of gravity in the flow direction, which increases with increasing inclination. Prior to onset of the thermal instability, the boundary layer is still laminar and largely two-dimensional, in which case enhancement may be attributed solely to the effect of gravity on the velocity and temperature profiles.

4.2. *Pre-instability*

In this section, data which indicate heat transfer enhancement prior to secondary flow are compared to the pre-instability numerical predictions. For a horizontal channel, the data in Fig. 10 are for the experimental conditions most conducive to pre-instability enhancement ($H = 60$ mm, $Re = 125$). These data were associated with larger experimental uncertainties because of low heat transfer coefficients and larger losses. Nevertheless, data for upstream regions of the plate at the lower heat fluxes are well correlated with z^* and show little effect of Grashof number, suggesting the existence of forced convection heat transfer. Data for the larger heat fluxes, on the other hand, show considerable enhancement which may be attributed to the induced streamwise pressure gradient.

Pre-instability heat transfer enhancement for the three largest Grashof numbers in Fig. 10 and for the inclined plate data of Fig. 9 are compared with predictions in Figs. 11(a) and (b), respectively. To reduce the effect of systematic experimental error, the comparison is made in terms of Nusselt numbers normalized with respect to measured forced convection values. Such normalization also reduces the effect of axial conduction, which is not modeled, on the comparison. Grashof numbers used for the calculations in Fig. 11 are based on the plate-averaged convective heat flux and fluid properties. Experimental data beyond the onset of secondary flow show a very rapid increase in the enhancement ratio because of three-

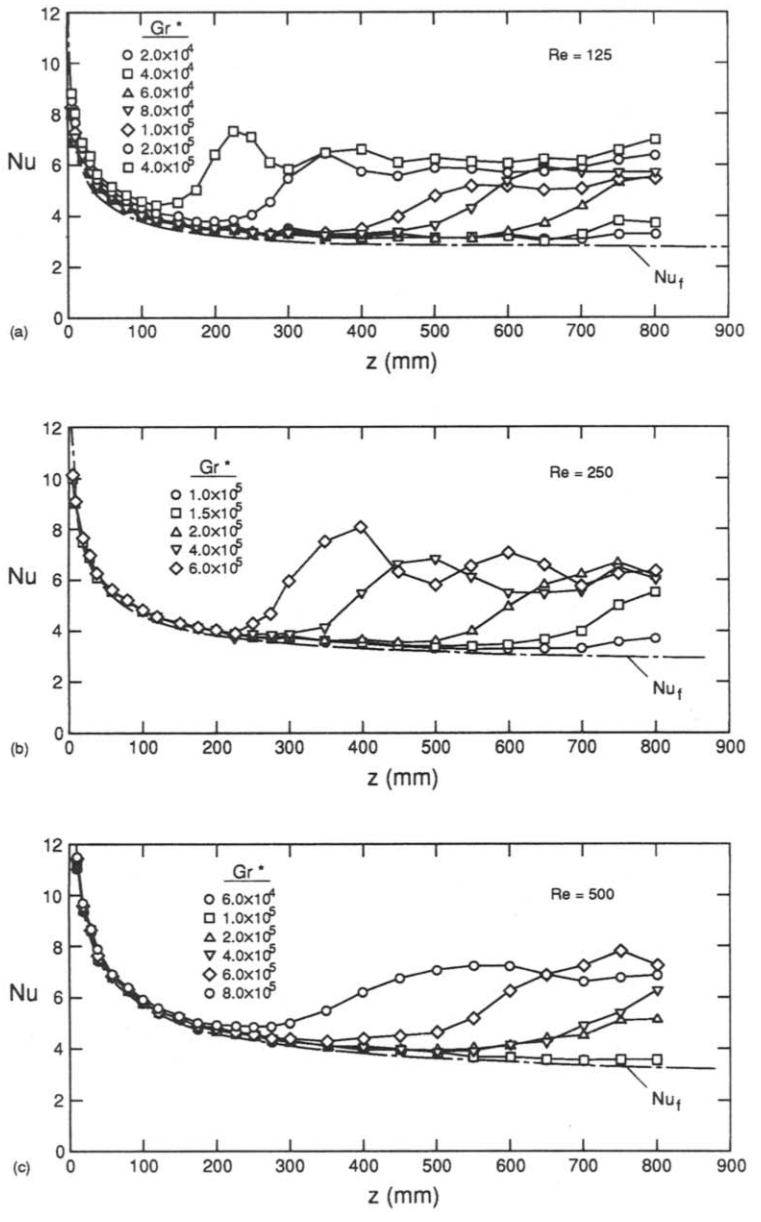

FIG. 7. Spanwise-averaged longitudinal Nusselt number distribution for $H = 30$ mm, $\theta = 0°$, $Pr = 0.7$: (a) $Re = 125$; (b) $Re = 250$; (c) $Re = 500$.

dimensional secondary flow and are not included in the figures.

Although the experimental uncertainty and the inability of the two-dimensional model to account for some aspects of the flow (sidewall plumes, for example) detract from the comparison of Fig. 11, the agreement is nevertheless reasonable. Despite differences in magnitudes, the calculations track the observed effects of axial distance, inclination angle, and plate heat flux, verifying the existence of pre-instability mixed convection effects.

4.3. *Fully developed and maximum Nusselt numbers*

Results from experiments which appeared to reach fully developed conditions are shown in Fig. 12(a), where the modified Rayleigh number is the average value over the portion of the plate in the fully developed region. Also included in the figure are data from ref. [9], which were obtained with a longer test section and were specifically intended to investigate fully developed flow. Clearly, increased heating drives a stronger secondary flow and increases the fully developed Nusselt number. For $Ra^* > 10^4$, the data are correlated by the expression, $Nu_{fd} = 0.30(Ra^*)^{0.25}$. The earlier data and the higher Ra^* data of this study are particularly well correlated, while the low Ra^* data of this study are slightly underpredicted. It is possible that the flows corresponding to this data were not completely fully developed, since secondary flows at low Rayleigh numbers develop slowly.

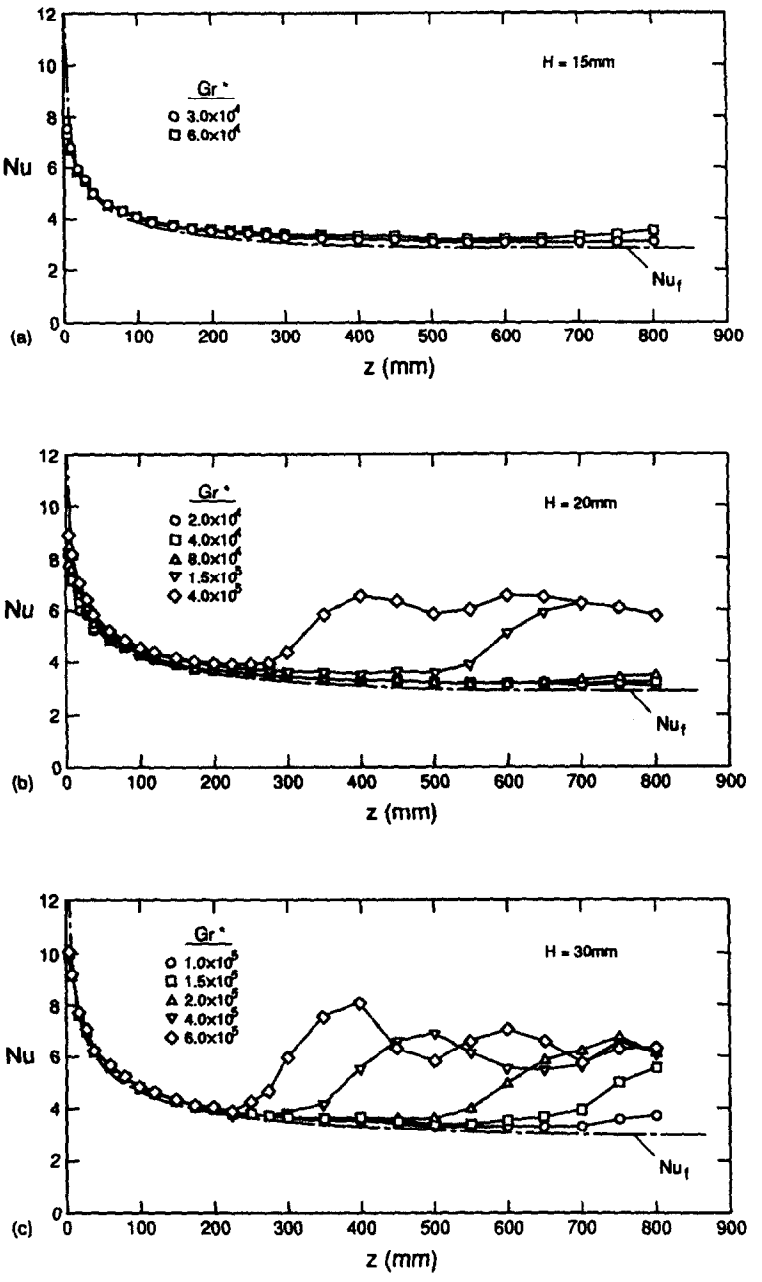

FIG. 8. Spanwise-averaged longitudinal Nusselt number distribution for $Re = 250$, $\theta = 0°$, $Pr = 0.7$: (a) $H = 15$ mm; (b) $H = 20$ mm; (c) $H = 30$ mm.

The maximum Nusselt number for each condition is also of interest, and values are plotted in Fig. 12(b), where the fully developed data, and the corresponding correlation are included for comparison. Although the maximum value increases with increasing Rayleigh number, it is not much higher (10–35%) than the eventual fully developed value, and approaches this value with increasing Rayleigh number. An important implication of this result is that, once the Nusselt number has reached its maximum value, there is little further change in the downstream direction. Hence, the value of the maximum Nusselt number is only slightly underpredicted by the correlation for the fully developed Nusselt number.

4.4. *Flow and heat transfer regimes*

The foregoing effects are summarized in Fig. 13, which delineates regions of forced convection and secondary flow for airflow in the thermal entry region of a parallel plate channel heated uniformly from below with $Re \leqslant 500$. Locations for the onset of secondary flow ($z^*_{c,f}$), the onset of heat transfer enhancement ($z^*_{c,h}$), and the maximum Nusselt number (z^*_{max}) are plotted against the local value of the modified

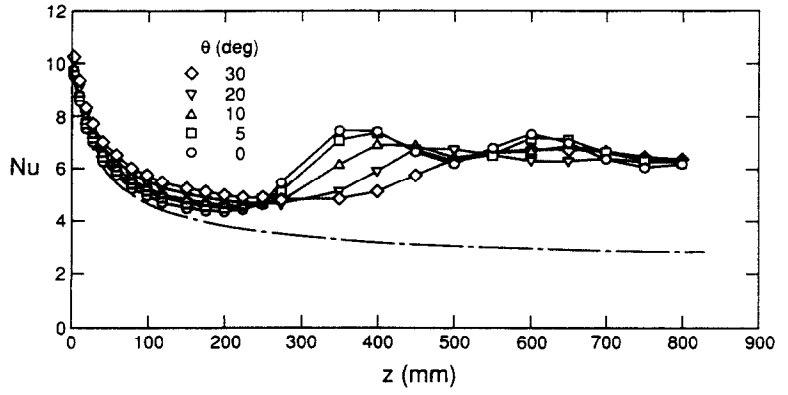

FIG. 9. Effect of inclination angle on longitudinal Nusselt number distribution for $Gr^* = 6 \times 10^5$, $Re = 250$, and $Pr = 0.7$.

Rayleigh number. Although z^* was not able to entirely collapse the experimental Nusselt number distributions [9], these results suggest that this parameter can scale the most important aspects of the flow. The suitability of z^* as a scaling parameter is reinforced by its appearance in the thermal instability equation [5] and by three-dimensional numerical results for different Reynolds numbers which collapse entirely with z^* [18]. Data showing the largest deviation from the curves (solid data symbols) are associated with significant pre-instability enhancement (large Gr^*/Re^2) and suggest that results where pre-instability enhancement is significant may not scale with Ra^* and z^* alone. These data were not used in developing the correlations.

For low values of z^* and Ra^*, laminar forced convection conditions are present, except for situations where large values of Gr^*/Re^2 may cause heat transfer enhancement (Figs. 1 and 2). At the location labeled as the onset of secondary flow, flow conditions are no longer uniform in the spanwise direction, which may be important in applications such as chemical vapor deposition. Overall enhancement in the spanwise-averaged heat transfer coefficient, however, does not occur until further downstream. Nusselt numbers on the plate between the onset of secondary flow and heat transfer enhancement can be predicted with laminar forced convection correlations. Beyond $z^*_{c,h}$, the exact behavior of the heat transfer coefficient cannot be correlated; however the location of the first maximum can be determined from the figure and the value of that maximum is expected to be roughly 10–30% higher than the fully developed Nusselt number predicted by $Nu_{fd} = 0.30(Ra^*)^{0.25}$. Furthermore, while the distance required to reach fully developed conditions cannot be predicted, variations in the heat transfer coefficient between the maximum and fully developed conditions are not extreme. Also note that, although transition to turbulent flow cannot be determined from the graph, such a transition is not associated with a sharp change in the Nusselt number. Thus, Fig. 13 provides a good indication of which regions

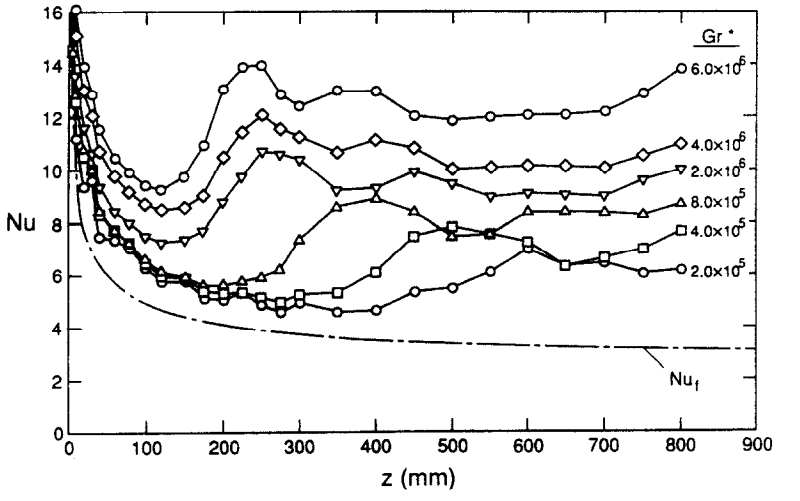

FIG. 10. Spanwise-averaged longitudinal Nusselt number distribution for $H = 60$ mm, $Re = 125$, $Pr = 0.7$, and $\theta = 0°$.

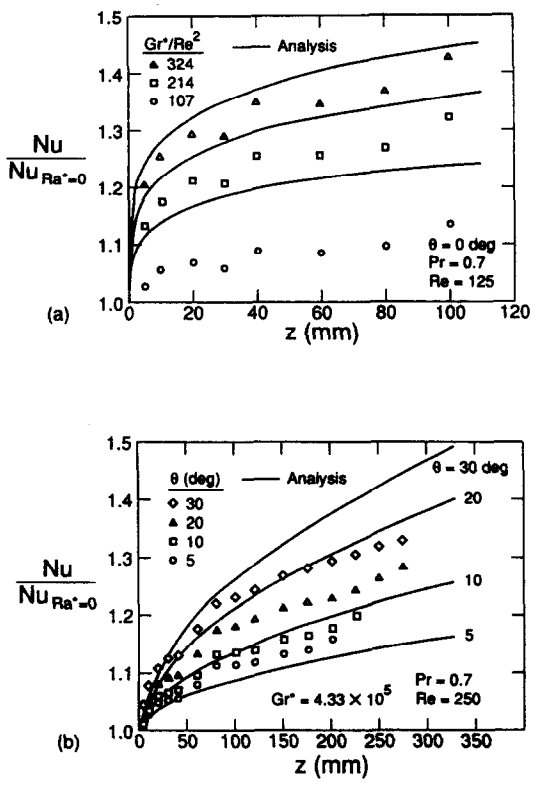

FIG. 11. Comparison of pre-instability analysis with experimental data for (a) horizontal and (b) inclined channels.

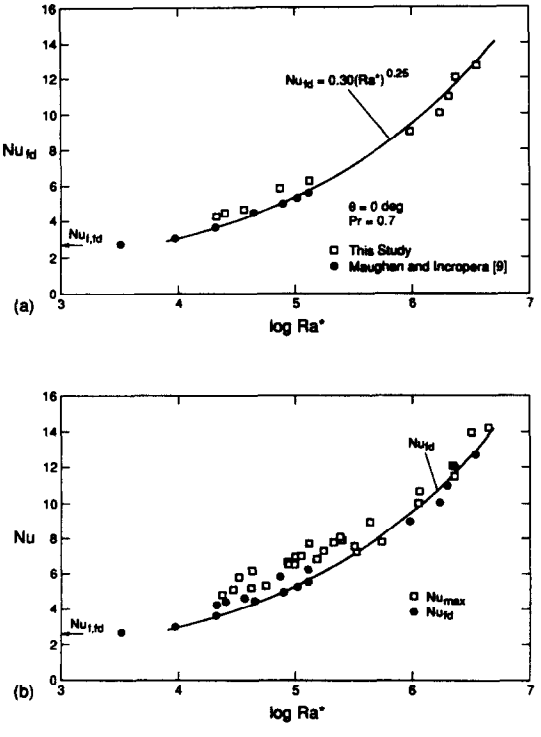

FIG. 12. Nusselt numbers for (a) fully developed conditions and (b) maximum values.

of a channel heated from below have secondary flow and how heat transfer in each region should be estimated. Equations for the correlations suggested in Fig. 13 are listed below

onset of secondary flow:

$$Ra^*_{c,f} = 1620(z^*_{c,f})^{-1.34} \tag{10}$$

onset of enhancement:

$$Ra^*_{c,h} = 2400(z^*_{c,h})^{-1.43} \tag{11}$$

maximum Nusselt number:

$$Ra^*_{max} = 1950(z^*_{max})^{-1.95}. \tag{12}$$

Results for the onset of secondary flow are compared to data from refs. [4, 6] in Fig. 14. A comparison to the previous work, which pertains to the onset of instability for airflow in the thermal entry region between isothermal plates (heated bottom plate, cooled top plate) is made possible by dividing the current critical modified Rayleigh numbers by the local Nusselt number, resulting in a Rayleigh number based on the temperature difference between the plate and the bulk fluid temperature. Although the current data show greater scatter when reduced in this fashion, the figure shows that the results for small to moderate Rayleigh numbers agree reasonably well with those of Kamotani *et al.* [4] for flow between isothermal plates, where the onset of instability was determined through flow visualization. That work, in turn, agrees well with the results of ref. [3] for similar conditions.

In ref. [6] the onset of instability was defined as the location where spanwise axial velocity profiles measured at $y/H = 0.2$ deviated 3.0% from the upstream condition. As shown in Fig. 14, these results do not scale well with z^*. Results for the lower Reynolds numbers had consistently larger values of z^*_c, particularly for the lower Rayleigh numbers. This behavior is attributed to the method of finding the onset of secondary flow. In particular, it might be expected that a lag would exist between the formation of a slight secondary flow and any detectable effect on the axial velocity distribution. Hence, data based on the velocity measurements reveal a delayed onset of secondary flow when compared to the earlier flow visualization data. Measurements of the vertical velocities, though more difficult, would be a better indicator. Note that the difference is greatest for low Rayleigh numbers, where the secondary flow develops more slowly.

5. SUMMARY

Several aspects of heat transfer enhancement in a parallel plate channel heated uniformly from below were investigated. Prior to thermal instability, flow acceleration caused by fluid expansion and the induced pressure gradient can enhance heat transfer. In an inclined channel, the streamwise component of

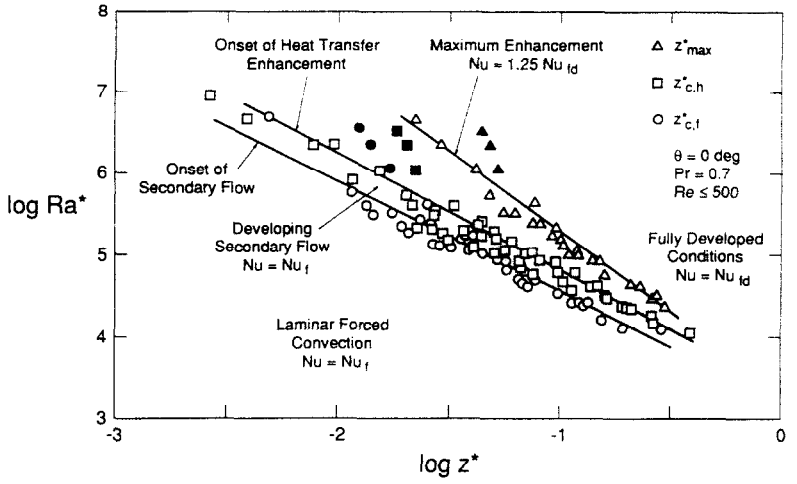

FIG. 13. Regions of developing secondary flow and heat transfer enhancement in a parallel plate channel.

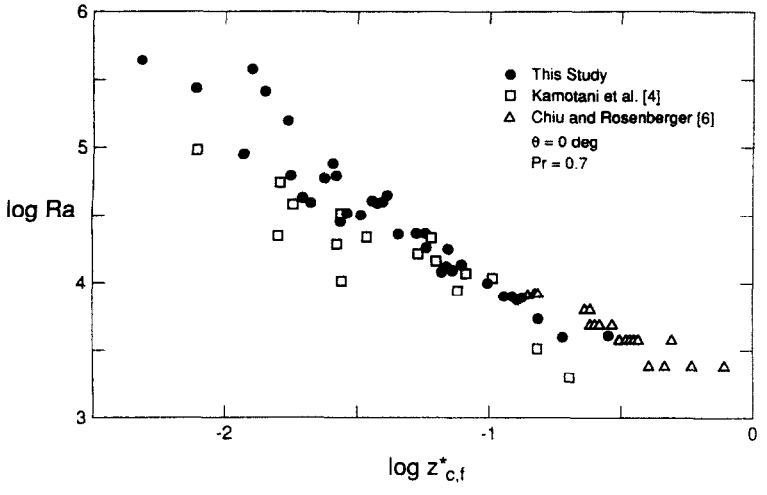

FIG. 14. Comparison of the data of this study for onset of secondary flow with results for flow between isothermal plates.

the buoyancy force can enhance heat transfer directly. Numerical computations were performed to predict the magnitude of each effect and showed that, for large heat fluxes and low flow rates, appreciable enhancement can occur before thermal instability.

Simultaneous heat transfer measurements and flow visualization were used to determine the effects of thermal instability on the flow. Experiments were performed over a wide range of flow conditions and results showed that significant heat transfer enhancement was preceded by the onset of secondary flow. Results were scaled with Ra^* and z^* and correlations were developed for the locations of the onset of secondary flow, the onset of heat transfer enhancement, and the maximum Nusselt number in a horizontal channel. Except for flows with large Gr^*/Re^2, heat transfer prior to the onset of enhancement may be predicted with forced convection correlations. This includes a region of developing secondary flow. Although Nusselt numbers between $z^*_{c,h}$ and z^*_{max} cannot be predicted, the value of the Nusselt number at z^*_{max} was generally found to be approximately 25% higher than the fully developed value. Furthermore, variations in Nu beyond z^*_{max} were small. As a result, Nusselt numbers downstream from the maximum value can be approximated with the correlation for fully developed flow, $Nu_{fd} = 0.30(Ra^*)^{0.25}$.

Acknowledgements—The support of the National Science Foundation under Grant No. CBT-8316580 is gratefully acknowledged. One author (J.R.M.) is also grateful for fellowships provided by Chevron Corporation, NL Industries Foundation, the Shell Foundation, and the Ingersoll Rand Corporation.

REFERENCES

1. Y. Mori and Y. Uchida, Forced convection heat transfer between horizontal flat plates, *Int. J. Heat Mass Transfer* **9**, 803–816 (1966).

2. S. Ostrach and Y. Kamotani, Heat transfer augmentation in laminar fully developed channel flow by means of heat from below, *J. Heat Transfer* **97**, 220–225 (1975).
3. G. J. Hwang and C.-L. Liu, An experimental study of convective instability in thermal entrance region of a horizontal parallel plate channel heated from below, *Can. J. Chem. Engng* **54**, 521–525 (1976).
4. Y. Kamotani, S. Ostrach and H. Miao, Convective heat transfer augmentation in thermal entrance regions by means of thermal instability, *J. Heat Transfer* **101**, 222–226 (1979).
5. G. J. Hwang and K. C. Cheng, Convective instability in the thermal entrance region of a horizontal parallel plate channel heated from below, *J. Heat Transfer* **95**, 72–77 (1973).
6. K.-C. Chiu and F. Rosenberger, Mixed convection between horizontal plates—entrance effects, *Int. J. Heat Mass Transfer* **30**, 1645–1654 (1987).
7. K.-C. Chiu, J. Quazzani and F. Rosenberger, Mixed convection between horizontal plates—fully developed flow, *Int. J. Heat Mass Transfer* **30**, 1655–1662 (1987).
8. F. P. Incropera, A. L. Knox and J. R. Maughan, Mixed convection flow and heat transfer in the entry region of a horizontal rectangular duct, *J. Heat Transfer* **109**, 434–439 (1987).
9. J. R. Maughan and F. P. Incropera, Experiments on mixed convection heat transfer for airflow in a horizontal and inclined channel, *Int. J. Heat Mass Transfer* **30**, 1307–1318 (1987).
10. J. R. Maughan and F. P. Incropera, Secondary flow in horizontal channels heated from below, *Exp. Fluids* **5**, 334–343 (1987).
11. E. Naito, The effect of buoyancy on laminar flow and heat transfer in the entrance region between horizontal parallel plates, *Int. Chem. Engng* **25**, 315–323 (1985).
12. E. M. Sparrow and W. J. Minkowycz, Buoyancy effects on horizontal boundary layer flow and heat transfer, *Int. J. Heat Mass Transfer* **5**, 505–511 (1962).
13. S. S. Moharreri, B. F. Armaly and T. S. Chen, Measurement in the transition vortex flow regime of mixed convection above a horizontal heated plate, *J. Heat Transfer* **110**, 358–365 (1988).
14. R. R. Gilpin, H. Imura and K. C. Cheng, Experiments on the onset of longitudinal vortices in horizontal Blasius flow heated from below, *J. Heat Transfer* **100**, 209–221 (1978).
15. N. Ramachandran, B. F. Armaly and T. S. Chen, Measurements of laminar mixed convection flows adjacent to an inclined surface, *J. Heat Transfer* **109**, 146–150 (1987).
16. S. V. Patankar, *Numerical Heat Transfer and Fluid Flow*. Hemisphere, Washington, DC (1980).
17. R. E. Lundberg, W. C. Reynolds and W. M. Kays, Heat transfer with laminar flow in concentric annuli with constant and variable wall temperature and heat flux, NASA TN-D-1975 (1963).
18. F. P. Incropera and J. A. Schutt, Numerical simulation of laminar mixed convection in the entrance region of horizontal rectangular ducts, *Numer. Heat Transfer* **8**, 707–729 (1985).

REGIONS D'ACCROISSEMENT DU TRANSFERT THERMIQUE POUR LA CONVECTION LAMINAIRE MIXTE DANS UN CANAL ENTRE PLAQUES PARALLELES

Résumé—On étudie l'acroissement de transfert thermique en convection mixte entre plaques parallèles avec chauffage uniforme par le bas. Des calculs numériques montrent l'accroissement de transfert thermique lié à l'instabilité thermique dans un canal horizontal, du fait de la dilatation du fluide et d'un gradient induit de pression et, dans un canal incliné, du fait de la composante de la pesanteur dans la direction de l'écoulement. Une visualisation et des mesures de transfert thermique, pour l'air en mouvement dans un canal horizontal, sont conduites dans un large domaine de conditions pour situer les régimes de convection forcée et mixte. On trouve qu'un écoulement secondaire précède un accroissement appréciable du transfert de chaleur. Excepté pour des grandes valeurs de Gr^*/Re^2, les nombres de Nusselt avant l'apparition de l'augmentation peuvent être prédits par des formules de convection forcée. Ensuite les nombres de Nusselt croissent rapidement vers une valeur maximale puis se fixent à une valeur qui est légèrement inférieure au maximum. Des formules sont proposées pour les nombres de Nusselt établis et pour les emplacements de l'écoulement secondaire, l'apparition de l'accroissement et le nombre de Nusselt maximal.

BEREICHE MIT ERHÖHTEM WÄRMEÜBERGANG BEI LAMINARER MISCHKONVEKTION ZWISCHEN PARALLELEN PLATTEN

Zusammenfassung—Untersucht wird die Erhöhung des Wärmeübergangs bei Mischkonvektion zwischen zwei parallelen Platten bei gleichförmiger Wärmezufuhr von unten. Numerische Berechnungen zeigen eine Erhöhung des Wärmeübergangs vor dem Auftreten einer thermischen Instabilität in einem horizontalen Kanal (infolge der Ausdehnung des Fluids und eines dadurch induzierten Druckgradienten) sowie in einem geneigten Kanal, wenn eine Komponente der Schwerkraft in Strömungsrichtung zeigt. In einem weiten Parameterbereich wird die Luftströmung in einem horizontalen Kanal sichtbar gemacht sowie der Wärmeübergang gemessen. Damit werden Gebiete erzwungener und gemischter Konvektion abgegrenzt. Der Beginn der Sekundärströmong leitet eine feststellbare Erhöhung des Wärmeübergangs ein. Außer bei großen Werten von Gr^*/Re^2 können die Nusselt-Zahlen vor dem Einsetzen der Erhöhung des Wärmeübergangs durch Korrelationen für erzwungene Strömung berechnet werden. Danach erhöht sich die Nusselt-Zahl sehr schnell bis zu einem Maximum und nimmt dann einen konstanten Wert an, der nur wenig geringer als der maximale Wert ist. Zwischen dieser Nusselt-Zahl und dem Ort des Einsetzens der Sekundärströmung sowie des Einsetzens der Erhöhung de Wärmeübergangs und der maximalen Nusselt-Zahl werden Korrelationen vorgeschlagen.

ОБЛАСТИ ИНТЕНСИФИКАЦИИ ТЕПЛООТДАЧИ ПРИ ЛАМИНАРНОЙ СМЕШАННОЙ КОНВЕКЦИИ В ПЛОСКОПАРАЛЛЕЛЬНОМ КАНАЛЕ

Аннотация—Исследуется интенсификация теплопереноса при смешанноконвективном течении между параллельными пластинами, равномерно нагреваемыми снизу. Численные расчеты показывают, что интенсификация теплопереноса предшествует возникновению тепловой неустойчивости, обусловленной в горизонтальном канале расширением жидкости и индуцированным градиентом давления, а наклонном канале—составляющей силы гравитации в направлении течения. С целью установления областей вынужденной и смешанной конвекции проведены визуализация течения и измерения теплопереноса для потока воздуха в горизонтальном канале для широкого диапазона условий. Найдено, что существенной интенсификации теплопереноса предшествует возникновение вторичного течения. Значения числа Нуссельта до начала интенсификации процесса можно рассчитать, за исключением больших значений Gr^*/Re^2, при помощи соотношений, полученных для случая вынужденной конвекции. Затем числа Нуссельта резко возрастают до максимума и после этого принимают установившееся значение, которое немного ниже максимального. Предложены соотношения для установившихся значений чисел Нуссельта, для положения областей возникновения вторичных течений и интенсификации теплоотдачи, для максимального значения числа Нуссельта.